RESEARCH PAPER

Vacuum Diffusion Bonding of Dissimilar Metal Alloys AA2219 and Ti-6Al-4V: Influence of Bonding Pressure on Microstructure and Mechanical Properties of the Bonding Joint

Manjunath Vatnalmath[1], Virupaxi Auradi[1], Bharath Vedashantha Murthy[2], Madeva Nagaral[3], Suresh Shetty[4], G B Veeresh Kumar[5,*]

** veeru232@gmail.com*

[1] Department of Mechanical Engineering, Siddaganga Institute of Technology, Tumakuru, affiliated to Visvesvaraya Technological University, Belagavi, Karnataka, India
[2] Department of Mechanical Engineering, RNS Institute of Technology, Bangalore, Visvesvaraya Technological University, Karnataka, India
[3] Aircraft Research and Design Centre, HAL, Bangalore-560037, Karnataka, India
[4] Department of Mechanical Engineering, Nitte (Deemed to be University), NMAM Institute of Technology (NMAMIT), Nitte-574110, Karnataka, India
[5] Department of Mechanical Engineering, National Institute of Technology–Andhra Pradesh, Tadepalligudem, Andhra Pradesh, India

Received: October 2024 **Revised: May 2025** **Accepted: June 2025**
DOI: 10.22068/ijmse.3776

Abstract: *Dissimilar joints of AA2219 and Ti-6Al-4V alloys are obtained using the vacuum diffusion bonding method. The bonding pressure is controlled in the 1-4 MPa range by keeping the bonding temperature and holding time constant. The influence of the bonding pressure on the microstructure and mechanical properties of the bonding joints is investigated. The diffusion behaviour across the interface of the bonding joints increases with the increase in bonding pressure. The interface morphology of the specimen bonded at lower bonding pressures exhibits scraggly voids and cracks. The irregular voids and cracks are squeezed and gradually closed due to the significant increase in the diffusion between Al and Ti. The maximum shear strength of 81 MPa is obtained for the joint made at the bonding pressure of 4 MPa, and a diffusion layer of 0.76 μm is formed at the Ti side interface. The fracture morphology inferred the brittle failure of the bonding joints due to the formation of intermetallic compounds like TiAl, $TiAl_2$, and $TiAl_3$ at the interface of Al and Ti.*

Keywords: *AA2219, Vacuum, Diffusion, Interface, Interface morphology, Fracture morphology, Microstructure, Mechanical property.*

1. INTRODUCTION

The aerospace and aviation industries seek cost reduction programs by utilizing new material technology. The monolithic structures integrate the functions of the individual components and are the best solutions to replace the riveted and built-up structures. An additional element of the cost reduction initiatives entails minimising the number of connections within the aircraft structure by enlarging individual components or implementing novel joining technologies instead of riveting [1, 2]. Aluminum (Al) alloys have been utilised extensively in commercial and military aircraft construction for nearly eight decades. This continued usage is attributed to their widely recognised mechanical properties, design simplicity, established manufacturing processes, and effective inspection techniques Aluminum Alloy (AA) 2219 is an Aluminum-Copper alloy, significantly used in propeller tanks and space boosters. It possesses excellent wear and corrosion resistance over other AA because copper is the main alloying element. Apart from this, it also has good formability and weldable properties, which support the healing of the cracks by accommodating more eutectics. However, conventional welding methods like fusion welding techniques cause the dissolution of the strengthening precipitates during melting and defects like porosity, slag inclusions, solidification cracks and distortion in the heat-affected zone [3-6]. In addition, the structural components of Titanium (Ti) and Al alloys are vital in the aerospace and defence sectors. These materials are also crucial in various fields, including transportation, structural engineering, aircraft manufacturing, the automobile industry, medical prosthetics, orthopaedic implants, dental implants, sports equipment, jewellery, and mobile devices. Joining these materials would

[DOI: 10.22068/ijmse.3776]

produce components with lightweight and high-strength properties [7]. Joining dissimilar metals is an essential requirement where the component, such as compressors and low pressure blisks, demands the hybrid properties specifically in aerospace and high tech industries [8].,s There are numerous new technologies, including brazing, friction welding, friction stir welding and explosive welding, for fabricating dissimilar joint configurations. However, these methods are costly and have certain limitations. The joint configuration is rigid, necessitating that the joining sections be cylindrical and of a small diameter for friction welding or thin for explosive welding. Friction stir welding also limits the thickness of the sections to be joined, and it is difficult to identify the defect at the joints produced [9, 10]. Currently diffusion welding/bonding is emerged as a possible technique for joining various metal alloys to create dependable connections between materials that are either comparable or dissimilar. A strong bond forms as surface oxides collapse, allowing atom diffusion, recrystallization, and grain development under moderate pressure, while preventing cracks, segregation, and stress distortion [11-14]. In diffusion bonding, primarily three parameters, bonding temperature, pressure and holding time, play a role in joining metal alloys. The bonding temperature is controlled in the range of 0.7-0.9 times the absolute melting of the base metal [15-17]. The need for bonding pressure is to obtain intimate contact and fill the interfacial voids by causing the plastic deformation of the surface asperities. The bonding pressure would be in the range of the yield strength of the base metals, and hence it assures no macroscopic deformation [18-20]. After the surfaces come into contact, it is necessary to allow sufficient holding or bonding time to close voids at the interface. Therefore, adequate bonding time is crucial. However, prolonged bonding time at high temperatures can lead to deformation, which becomes uncontrollable after creep at the interface [21]. The diffusion bonding is usually carried out in a vacuum or an inert atmosphere to avoid oxidation and to produce metallurgically pure joints [22]. Diffusion bonding of Al and Ti alloys proves challenging due to the persistent oxide formation on the Al and the significant differences in thermal and mechanical properties between the two metals. Rajakumar et al. [23] developed an empirical relationship for predicting the lap shear strength, interlayer thickness, and weld interface hardness of the diffusion bonded AA7075 and pure Ti. The bonding parameters are optimized using Response Surface Methodology (RSM) to achieve elevated properties at the joints. The results of this study found that bonds formed at the bonding temperature of 510°C, pressure of 17 MPa, and holding time of 37 minutes exhibited maximum shear strength of 87 MPa, hardness of 163 HV, and interface layer thickness of 7 μm. Formation of Al_3Ti, AlTi and $AlCu_2Ti$ intermetallic compounds. Akca et al. [24] expounded on the diffusion bonding of Ti-6Al-4V alloy and commercially pure Al. Various welding parameters, such as varying bonding temperature in the range of 560-640°C, holding time between 30-60 minutes and constant bonding pressure of 3 MPa, are employed to improve the suitability of the materials for industrial applications. The results showed that the hardness values at the transition zone were higher than the Al side, but lower than the Ti side. Furthermore, the highest tensile strength is observed at the bonding temperatures of 640°C with a holding time of 60 min. Wei et al. [25] produced the diffusion bonded joints of pure Ti and Al to examine the bonding strength. The study utilized the constant bonding pressure of 5 MPa, larger holding time between 10-600 min and elevated temperature in the range of 500-650°C and the results suggested to that the specimen bonded at 650°C under the holding time of 600 min exhibited maximum shear strength near to that of pure Al. Jiangwei et al. [26] developed diffusion bonded joints of pure Ti and Al by Aluminizing the Ti surface to facilitate good diffusion across the interface. It was found that intermetallic like $TiAl_3$ and TiAl formed at the interface of the aluminized coating and Ti at the bonding temperature of 640°C, pressure of 24 MPa and holding time of 90 minutes. Besides, Akca [24], Wei [25] and Jiangwei [26] utilized a higher bonding temperature of more than 90% of the melting point of pure Al, which is more concerning for the plastic deformation of the Al base metals during diffusion bonding. Various combinations of temperature, pressure, and time can be utilised to achieve a strong metallurgical bond between different metals. These combinations of parameters would not depend on the structure being manufactured [27]. However, the parameters to be adhered to are the solidus temperature and

[DOI: 10.22068/ijmse.3776]

yield strength of the base metal, which has lower melting temperature and strength constituents, to get good metallurgical bonds. Moreover, vacuum diffusion bonding for engineering applications demands low temperature, low pressure and less holding times to fend off infelicitous phase transformations, significant deformations and grain coarsening [28]. In this context, more studies on diffusion bonding of Al and Ti alloys need to be investigated to reveal the feasibility and efficacy of the method. The current study attempts to join AA2219 and Ti-6Al-4V using diffusion bonding techniques which have not been reported hitherto. The microstructural and mechanical properties are evaluated for different bonding pressures. Furthermore, the influence of bonding pressure on the microstructure and mechanical properties of the bonding joints is discussed.

2. EXPERIMENTAL PROCEDURES

AA2219 (0.06% Ti, 0.01% Mg, 0.49% Si, 0.23% Fe, 0.2% Zr, 0.32% Mn, 6.48% Cu, 0.18% Zn 0.06% V, Bal.-Al) and Ti-6Al-4V (0.056% C, 0.29% Fe, 3.75% V, 5.68% Al, Bal.–Ti) are utilized to produce dissimilar metal joints using diffusion bonding. AA2219 and Ti-6Al-4V alloys are cut into the specific dimensions ($50 \times 50 \times 5$ mm^3) using wire cut Electric Discharge Machining (EDM). The surfaces of the geometrically prepared specimens are mechanically ground with various abrasive papers (#80, #220, #320, #400, #600, #800, #1000, and #1500). Fig. 1(a) and (b) show the optical microstructural images of base metals AA2219 and Ti-6Al-4V, respectively. Al alloys usually have low oxygen solubility and high oxygen stability, which poses difficulties during diffusion bonding. On the other hand, Ti alloys have high oxygen solubility, and the oxide layer gradually dissolves at elevated temperatures [29]. However, the bonding surfaces of AA2219 and Ti-6Al-4V are cleaned with chemical solutions to inhibit the defects caused by oxide formation during diffusion bonding. The AA2219 surfaces are washed with 6% NaOH and 40% HNO_3. Likewise, the bonding surfaces of Ti-6Al-4V are washed with 3% HF and then with 30% HNO_3 [25]. Chemically washed surfaces are then ultrasonically cleaned with acetone and dried using hot air before conducting the diffusion bonding.

The diffusion bonding is carried out in a furnace for various combinations of bonding pressure by keeping the constant bonding temperature and holding time of 540°C and 60 minutes, respectively. The vacuum of 7×10^{-4} Torr and heating rate of 10°C/min are maintained during the bonding process. Table 1 shows the various bonding parameters for the current diffusion bonding of AA2219 and Ti-6Al-4V. The bonding parameters are controlled using a control panel attached to the bonding furnace, and once the bonding temperature reaches 540°C, the bonding pressure is applied for the specified holding time. Fig. 2 depicts the schematic of the bonding furnace and photographic views of the bonded specimen, shear test specimen and shear die.

Fig. 3 shows the process cycle utilized during the diffusion bonding of AA2219 and Ti-6Al-4V. Once the bonding process is completed, the samples are cooled in the furnace itself to constrain the thermal defects on the bonded joints.

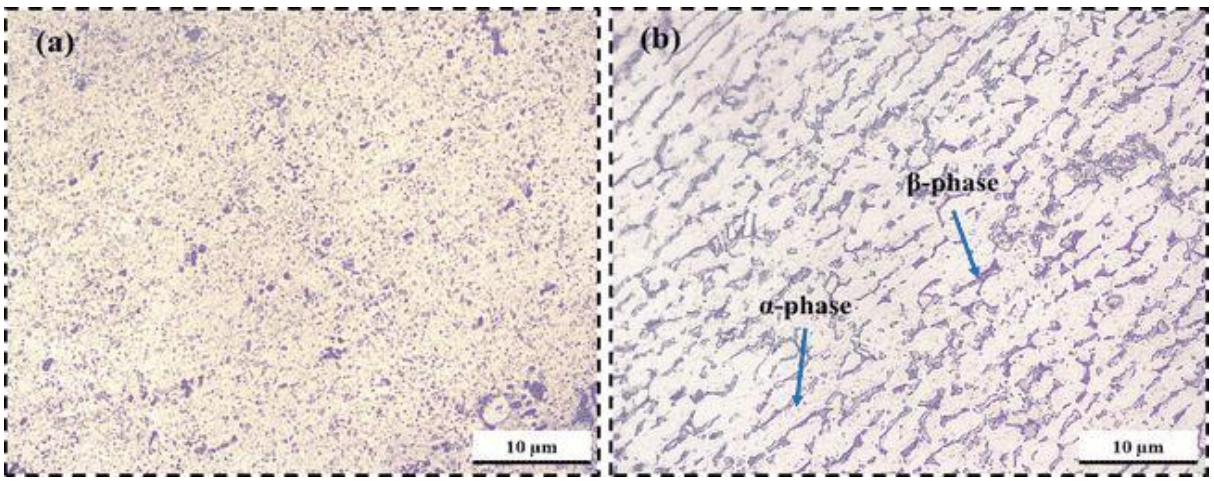

Fig. 1. Optical microstructure images of a) AA2219 and b) Ti-6Al-4V

[DOI: 10.22068/ijmse.3776]

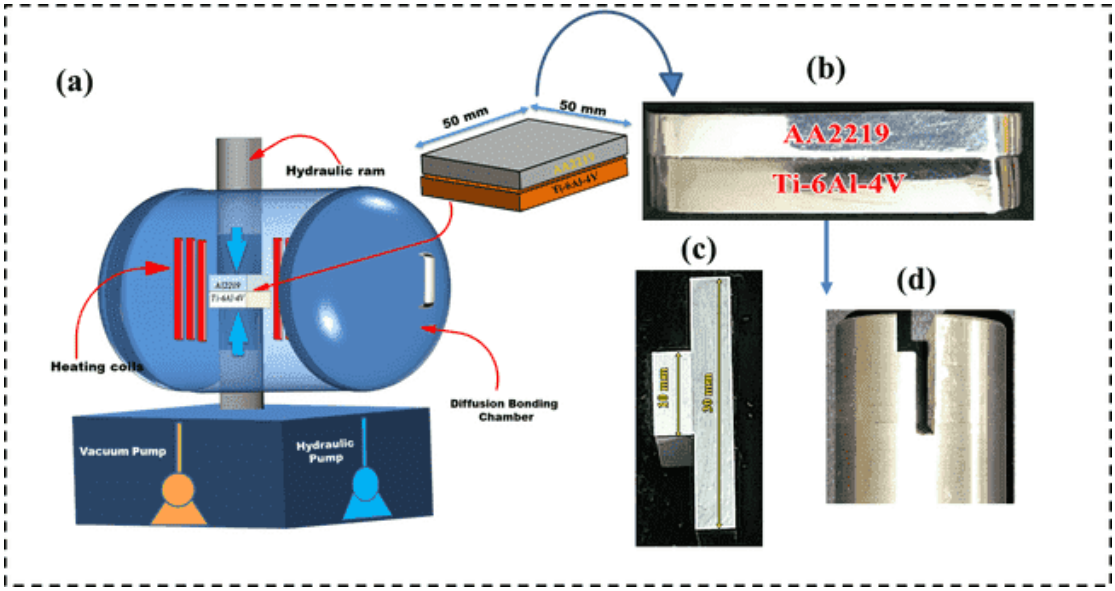

Fig. 2. a) schematic illustration of the bonding furnace, b) photographic view of the bonded specimen, c) photographic view of the specimen prepared for shear test, d) shear test die

Table 1. Diffusion bonding parameters

Pressure (MPa)	Time (Minutes)	Temperature (°C)
1	60	540
2	60	540
3	60	540
4	60	540

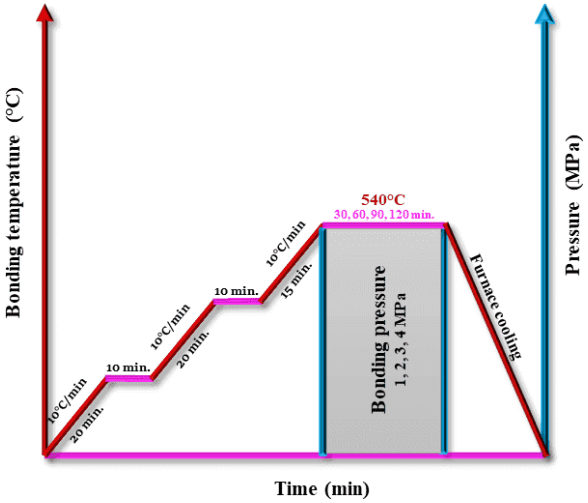

Fig. 3. Process cycle utilized for the diffusion bonding

The bonded samples are then cut perpendicularly to the joint interface using wire EDM, and the produced samples are prepared for the microstructure evaluation by grinding and polishing with various grades of grit papers (220-2000) and diamond paste (1 µm). The polished samples are then etched with Keller's reagent [30] (AA2219 side) and Kroll's reagent [31] (Ti-6Al-4V side), water flushed and dried using hot air. The microstructure and elemental analysis are carried out at the joint interface using SEM (Zeiss Gemini ULTRA 55), EDS (ULTR 55), and XRD (Panalytical X'Pert³). The bonding strength is evaluated using a shear test (BiSS-25 kN) at room temperature conditions with the crosshead speed of 1 mm/min. Microhardness (MICROMACH) measurement according to ASTM E384 is made with an indentation load of 50 gm and a dwell period of 15 sec.

3. RESULTS AND DISCUSSION

3.1. Interface Morphology

Fig. 4 shows optical microscopic images of the interface of the specimens produced at various bonding pressures. The specimen produced at the pressure of 1 MPa (Fig. 4a) and 2 MPa (Fig. 4b) shows an uneven interface accompanied by continuous, long, scraggly voids. However, the specimens produced at 3 MPa (Fig. 4c) and 4 MPa (Fig. 4d) unveil the interface without irregularity. Furthermore, the SEM examination is carried out to study the interface area of the bonded specimens in detail. The SEM micrographs of the specimens bonded at different bonding pressures are shown in Fig. 5. The specimen produced at the pressure of 1 MPa (Fig. 5a) exhibits an original bonding line along with a long, scraggly void, measuring an average thickness

[DOI: 10.22068/ijmse.3776]

of 0.8 µm. As the pressure increased to 2 MPa (Fig. 5b) and 3 MPa (Fig. 5c), the long, scraggly voids crushed to form thin penny-shaped voids and bonding zones at the interface. This stipulates the grain boundary migrations across the bonding line. The lower bonding pressures are inadequate to ensure intimate contact at the Al-Ti interface and lead to poor atomic transportation. When the bonding pressure increased to 4 MPa (Fig. 5d), the penny-shaped voids transformed into minute elliptical and spherical voids. In addition, a diffusion layer of 0.7 µm is observed towards the Ti side. Formations of the minute voids near the Al-rich layer are caused by the Kirkendall effect, allowing the diffusion of Al atoms into the Ti side through the Al rich layers [32]. Void shrinkage is an inevitable process that produces high-quality joints. During direct diffusion bonding, the bonding specimens encounter a plastic deformation on the bonding surfaces and asperities under axial stress. The asperities are then crushed to generate the interfacial gaps, leaving residual voids along the bonding line [33, 34]. Line scan EDS is used to analyse the diffusion behaviour of the elements across the interface zone. Fig. 6 shows point EDS and line scan EDS across the interface of the specimens bonded for various bonding pressures. The interface of all the bonding specimens consists of both Al and Ti elements, congruent with the point EDS analysis. The point EDS analysis on the interface of the specimen bonded at 1 MPa (Fig. 6a-1) has 74.37 at% of Al and 24.37 at% of Ti, and the line scan (Fig. 6b) shows the diffusion behaviour across the interface, and it is measured to 1.2 µm. At the bonding pressure of 2 MPa (Fig. 6c-1), the interface discloses the presence of Al with 54.06 at% and Ti of 44.07 at%, and the line scan (Fig. 6d) shows the diffusion zone, which is estimated to be 1.8 µm. When the bonding pressure increased to 3 MPa, the diffusion zone of 2.2 µm (Fig. 6f) is imparted with the presence of Al with 35.28 at% and Ti with 62.13 at% (Fig. 6e-1). Furthermore, increased bonding pressure to 4 MPa improved the diffusion behaviour between Al and Ti elements across the interface. A reaction layer (Fig. 5d) is observed near the interface at the Ti side and exhibits 74.56 at% of Al and 24.16% of Ti (Fig. 6g-1), stipulating the formation of $TiAl_3$ phase intermetallic and further the line scan EDS (Fig. 6h) shows a broader diffusion zone of about 3 µm. The increase in diffusion zone and the quality of the joint interface are mainly attributed to the increase in bonding pressure. Diffusion kinetics is determined by the temperature-dependent Arrhenius equation [35], which is depicted in equation 1.

$$D = D_o \exp(-Q/RT) \quad (1)$$

D is the diffusion coefficient, D_o is the pre-exponential factor, R is the gas constant, and T is the bonding temperature. In addition, the diffusion zone thickness relies on the diffusion bonding time and the diffusion coefficient (equation 2).

$$x = k\sqrt{Dt} \quad (2)$$

Where x is the thickness of the diffusion zone, and t is the bonding time. However, the bonding pressure also has an influence on the diffusion zone thickness. The EDS line scan shows the diffusion zone thickness increases with increased bonding pressure. From equations 1 and 2, at the bonding pressure of 1 MPa, the D is determined to be 4×10^{-16} m^2/s and similarly, at 4 MPa it is 2.5×10^{-15} m^2/s. This elucidates that the increase in bonding pressures caused the diffusion of more Al atoms towards the Ti side. According to Assari and Eghbali [36] the application of uniform bonding pressure would produce high quality joints between Al and Ti, which are produced by preventing the formation of cracks and voids.

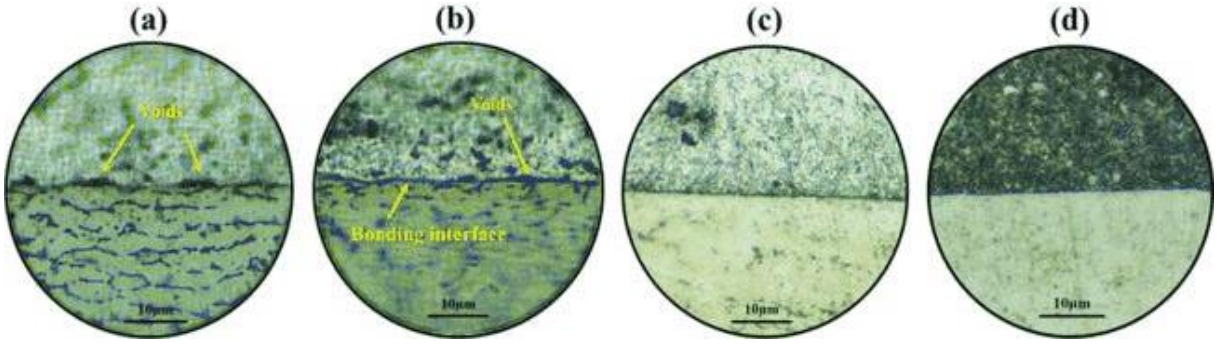

Fig. 4. Optical Micrographs of the specimen bonded at a) 1, b) 2, c) 3 and d) 4 MPa

[DOI: 10.22068/ijmse.3776]

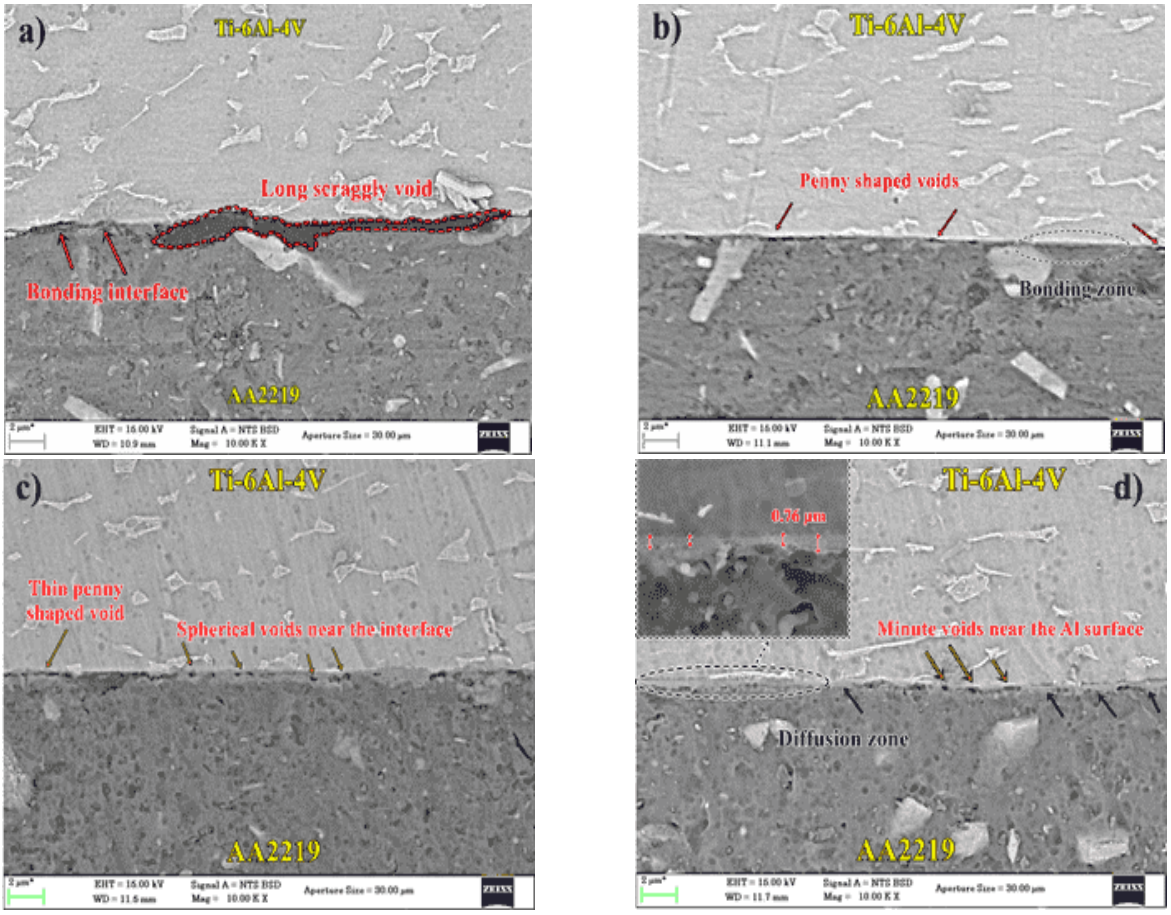

Fig. 5. SEM images of the bonded specimens for various bonding pressures a) 1 MPa b) 2 MPa c) 3 MPa d) 4 MPa

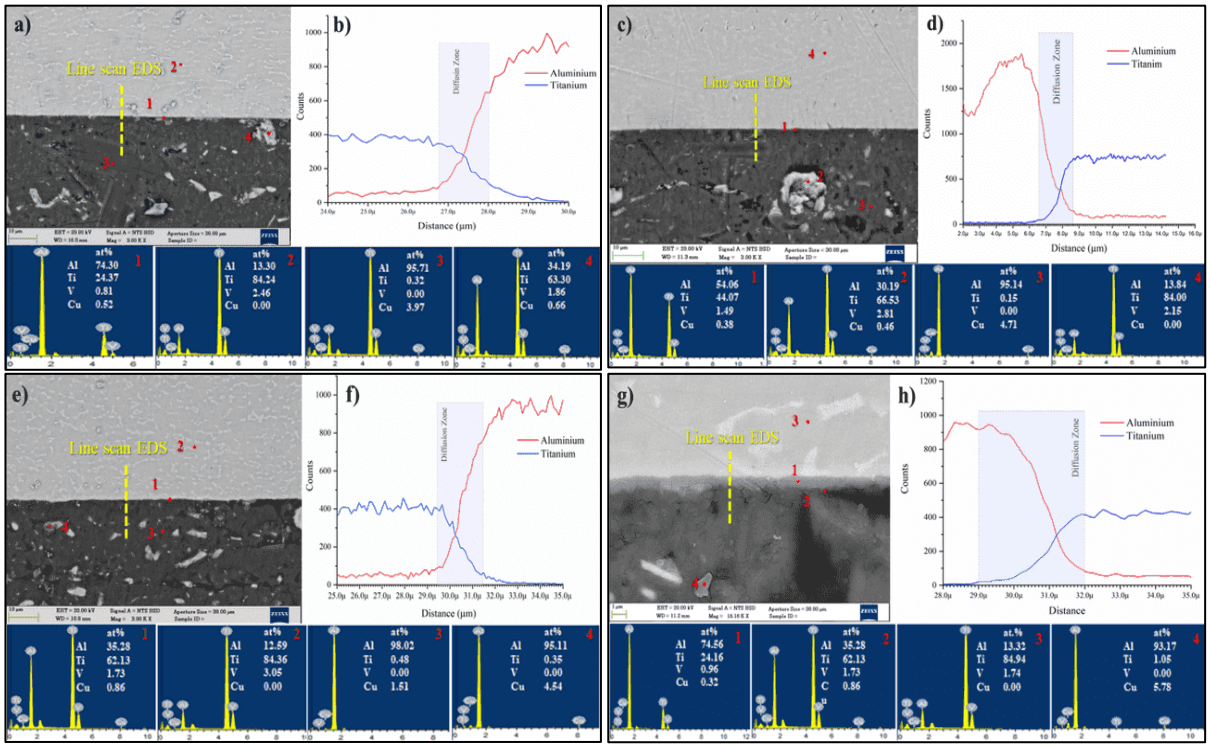

Fig. 6. Point and Line scan EDS results for the specimens bonded at a-b) 1 MPa, c-d) 2 MPa, e-f) 3 MPa, and g-h) 4 MPa

[DOI: 10.22068/ijmse.3776]

Kecskes et al. [37], in their study on the cold-rolled Ni/Al and Ti/Al multilayers, depicted the equilibrium phase diagram of Al-Ti, which shows the formation of $TiAl_3$, $TiAl_2$, TiAl, and Ti_3Al and other non-equilibrium phases like Ti_3Al_5. The intermetallic compound $TiAl_3$ has the least free energy compared to the other intermetallics like Ti_3Al, TiAl, and $TiAl_2$. Hence, the $TiAl_3$ generates and precipitates predominantly at the interface of Ti and Al when these elements reach their solid solubility. Moreover, the solubility of Al in Ti is 12%, whereas the solubility of Ti in Al is just 0.12% [38, 39]. Hence, the diffusion study of the Al-Ti system is complex, and more research is needed. The diffusion in metal alloys is generally based on two fundamental concepts: 1) understanding the transport mechanism of atoms and 2) determining the diffusion coefficients for the defined mechanism. The diffusion in most metals and alloys occurs through single vacancies, making near jumps. Plastic deformation acts as a catalyst for initiating defect nucleation, creating new diffusion paths by introducing lattice distortions [40, 41].

3.2. Mechanical Properties

3.2.1. Microhardness

Fig. 7(a) and (b) show the Microhardness profile of the bonding joints formed at various bonding pressures and the microhardness of the bonded joints as a function of bonding pressure, respectively. Microhardness is tested across the interface of the bonded specimens at an interval of 100 µm from the joint. The interface of the specimen bonded at 1 MPa exhibits a hardness value of 148.59 HV. The hardness at the joint is increased to 173.94 HV with an increase in bonding pressure to 4 MPa. Hardness value at the Ti side interface varies in the range of 357 to 367 HV, and it is increased to 431 HV when it is measured away from the interface. Whereas, the near interface of the Al side shows hardness values in the range of 69 to 73 HV, and away from the interface, it is decreased to 66 to 63 HV. It is observed that the width of the joint section is decreased. The hardness value increases at the interface of the bonding joints with increased bonding pressure. It is mainly attributed to the closure of cracks and voids and the formation of intermetallic compounds due to the significant diffusion of Al atoms into the Ti side. The change in microstructure and elemental composition at the interface would impact the mechanical properties of the associated regions [42].

3.2.2. Shear strength

Fig. 8 shows the shear strength of the bonding specimens as a function of bonding pressure. The shear strength of the joints produced at various bonding pressures is evaluated using the following formula [43].

$$\tau = \frac{P}{l \times w} \quad (1)$$

Where P is the applied shear load and l and w are the length and width of the shear test specimen at the interface. A minimum shear strength of 22.4 MPa is observed for the joint produced at the bonding pressure of 1 MPa. Furthermore, the shear strength increased with increased bonding pressure, and the joint produced at the bonding pressure of 4 MPa exhibits a maximum shear strength of 81 MPa.

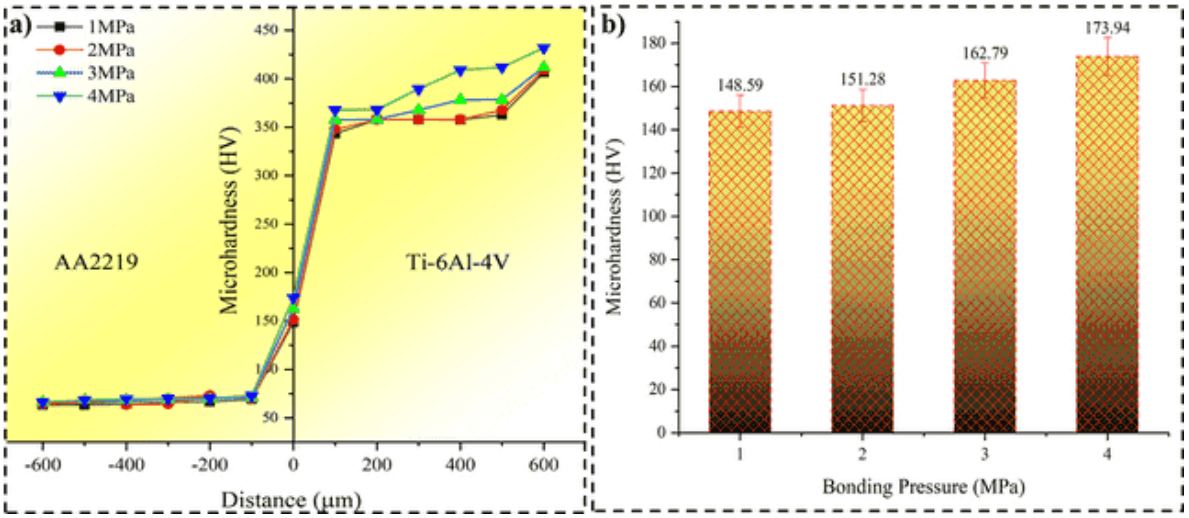

Fig. 7. a) Microhardness profile across the bonding joints b) Joint hardness as a function of bonding pressure

[DOI: 10.22068/ijmse.3776]

The shear strength curve (Fig. 8) has a sharply increasing trend up to the bonding pressure of 3 MPa, and then the curve gradually decelerates. The drop in shear strength at the lower bonding pressure is due to the minimum contact rate at the contacting surfaces. However, the increased plastic deformation and the diffusion rate at the elevated bonding pressure cause the rapid movement of atoms across the interface and are the reason for higher shear strength [44]. The increased shear strength can also be attributed to the formation of intermetallics.

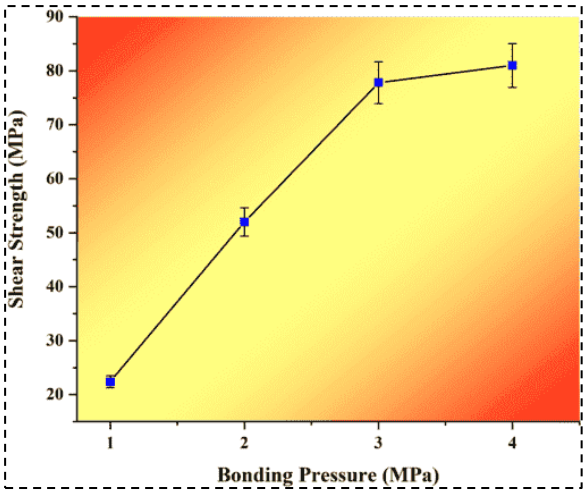

Fig. 8. Shear strength of the bonding joints as a function of bonding pressure

3.2.3. Fracture morphology

Failure analysis of the fractured surfaces is carried out after the shear test. Fig. 9 shows the fracture morphology of the joint interfaces bonded in the 1-4 MPa pressure range. All the joints are aligned at the bonding interface as the shear load is applied along the bonding line. The fracture morphology of the bonding joint made at 1 MPa (Fig. 9a-b) and 2 MPa (Fig. 9c-d) shows a flat fractured surface with minimum features at the Ti side, whereas the Al side shows the voids, shallow dimples, inclusions and crack initiation zone are developed due to the inadequate diffusion under the minimum bonding pressures and lack of commingle at the joining surfaces. The EDS analysis is carried out on Al and Ti fractured surfaces to know the elemental composition, further supporting the study of the intermetallic formed at the contacting surfaces. The results of EDS analysis are presented in Table 2. The point EDS on the spot 2 (Fig. 9b) has Al (73.87%) and Ti (23.96%), suggesting the formation of the $TiAl_3$ phase. However, the point EDS on spot 4 (Fig. 9d) contains the Al (66.99%) and Ti (32.81%), which specify the formation of $TiAl_2$ in addition to $TiAl_3$. Furthermore, the voids and crack initiation zones are reduced with increased bonding pressure to 3 MPa and 4 MPa. However, brittle failure is observed at the interface with cleavage facets, dimples, tear ridges, striations (Fig. 9e) and white regions (Fig. 9g-h) at Al and Ti sides [46]. The bright regions appear silvery white with black substrate behind (Fig. 9g-h) due to the formation of intermetallics between the Al and Ti. The point EDS on the spot 6 (Fig. 9f) has Al (44.78%) and Ti (55.22%), and on the spot 8 (Fig. 9h) shows the presence of Al (39.85%) and Ti (55.19%), suggesting the formation of TiAl in addition to the formation of $TiAl_2$ and $TiAl_3$. At reduced pressures (1–2 MPa), the fracture surfaces exhibited regions where cracks initiated and shallow dimples. However, the presence of $TiAl_3$ and $TiAl_2$ led to brittle crack propagation. At elevated pressures of 3–4 MPa, SEM images exhibited characteristics like cleavage facets, tear ridges, and luminous intermetallic areas. A continuous intermetallic compound layer observed at the specimen interface bonded at 4 MPa has more Al and Ti (Fig. 6g), stipulating the presence of Al_3Ti. According to Song et al. [45], the Al_3Ti is more brittle and harder than other Al-Ti intermetallics. The inherent high hardness and poor fracture toughness of these intermetallic compounds resulted in the development of weak planes, which acted as loci for crack initiation, promoting rapid crack propagation along the interface.

Table 2. Presents the EDS analysis results of the joint

Spot No. (Fig. 9)	Elements (%)		
	Al	Ti	Cu
1	93.71	4.04	2.25
2	73.87	23.96	2.17
3	98.78	0.16	1.06
4	66.99	32.81	0.20
5	98.72	0.00	1.28
6	44.78	55.22	0.00
7	90.05	3.64	6.31
8	39.85	55.19	4.96

The fracture morphology suggests that the fracture at the higher bonding pressure occurred at the interface of AA2219 and Ti-6Al-4V, where

[DOI: 10.22068/ijmse.3776]

intermetallic compounds like TiAl, $TiAl_2$, and $TiAl_3$ are formed. The fractured surfaces are further analysed through XRD using Panalytical X'Pert³. XRD diffraction patterns for the fractured surfaces made at different bonding pressures are shown in Fig. 10.

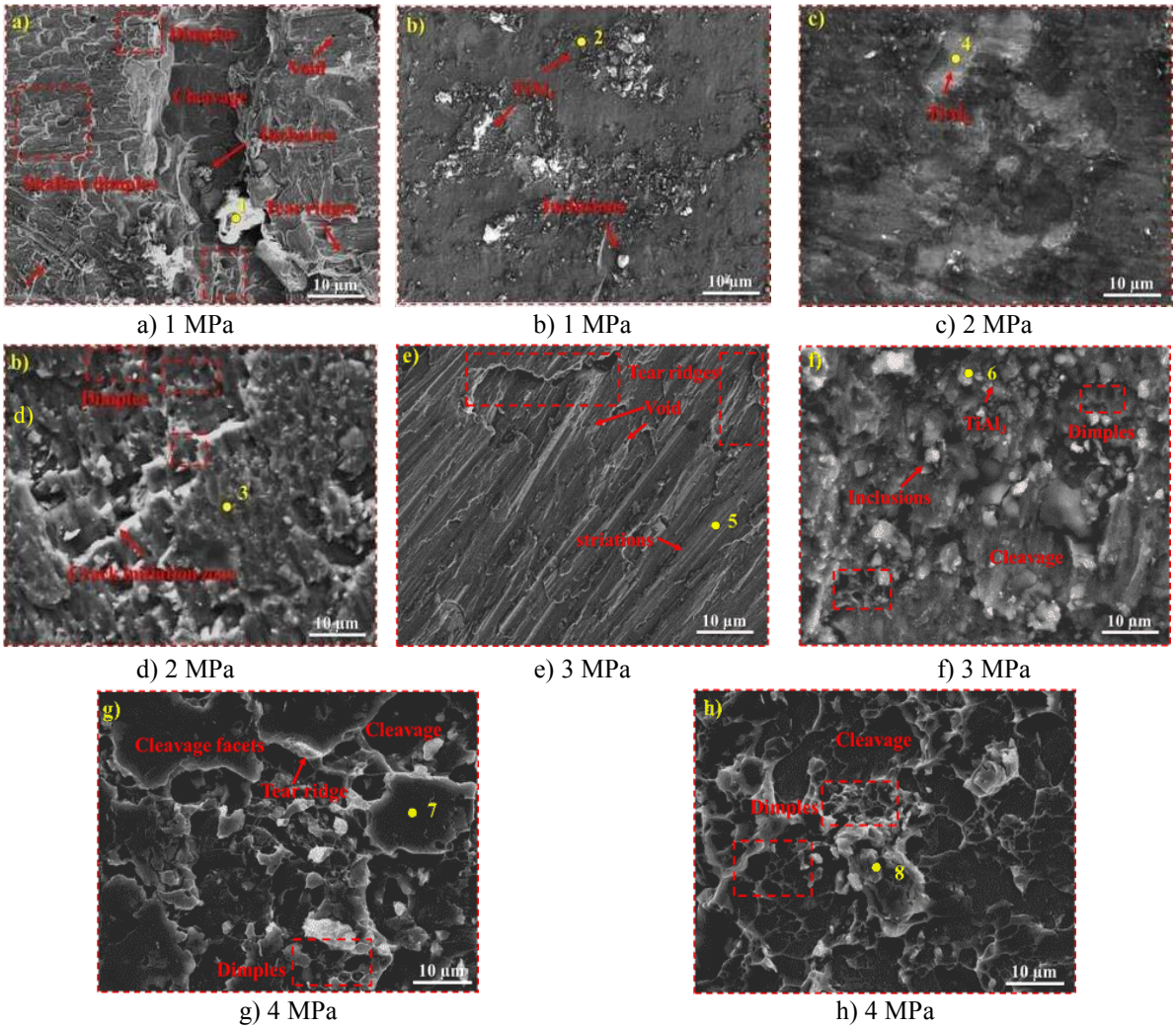

a) 1 MPa b) 1 MPa c) 2 MPa

d) 2 MPa e) 3 MPa f) 3 MPa

g) 4 MPa h) 4 MPa

Fig. 9. Fractography images of joints bonded for various bonding pressures (a, b)

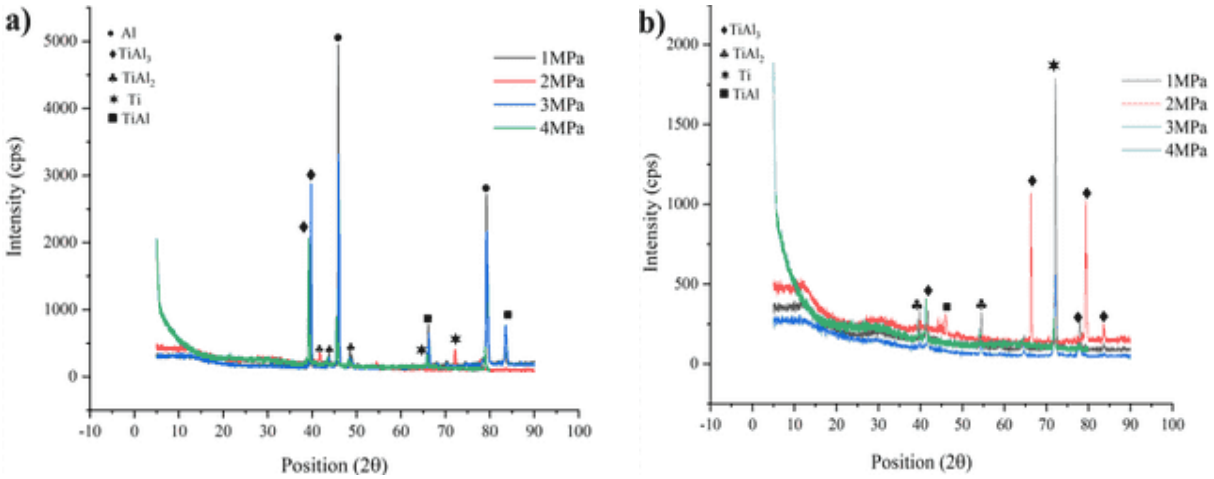

Fig. 10. XRD pattern for the fractured surfaces bonded at different bonding pressures a) Al side b) Ti side

[DOI: 10.22068/ijmse.3776]

The peaks illustrate the formation of TiAl, $TiAl_2$, and $TiAl_3$ intermetallics along with Al and Ti. However, the fractured surfaces at Ti do not show Al peaks, suggesting the formation of a diffusion layer towards the Ti side during diffusion bonding.

4. JOINT FORMATION MECHANISM

According to the microstructure analysis, the diffusion between Al and Ti occurs near the solidus temperature of the AA2219 with higher bonding pressure. Fig. 11 illustrates the forming mechanism for the bonding joint between AA2219 and Ti-6Al-4V. When the diffusion bonding process initiates, the asperities of the base metals contact primarily, and the elevated temperature makes these asperities on the Al side crush quickly compared to those on the Ti side (Fig. 11a). The difference in the yield strength produces cracks, large and scraggly voids at the interface. Further increase in the bonding pressure causes the plastic deformation at the contacting surfaces of Al and Ti, and the creep phenomenon predominately takes a further role in the joint formation mechanism. At this stage, (Fig. 11b, and c), the scraggly voids and cracks are crushed to form the elliptical and spherical voids. The diffusion of Al atoms initiates at the interface as the diffusion rate of Al in Ti is higher compared to the diffusion rate of Ti in Al. However, the atomic vibration due to the applied bonding temperature activates the motion of Ti atoms. Kirkendall void formation at the Al side interface creates the pathways for further diffusion of Al atoms. In addition, the bonding zone and a diffusion layer (Fig. 11d) are formed at the interface with good intimate contact between the Al and Ti surfaces.

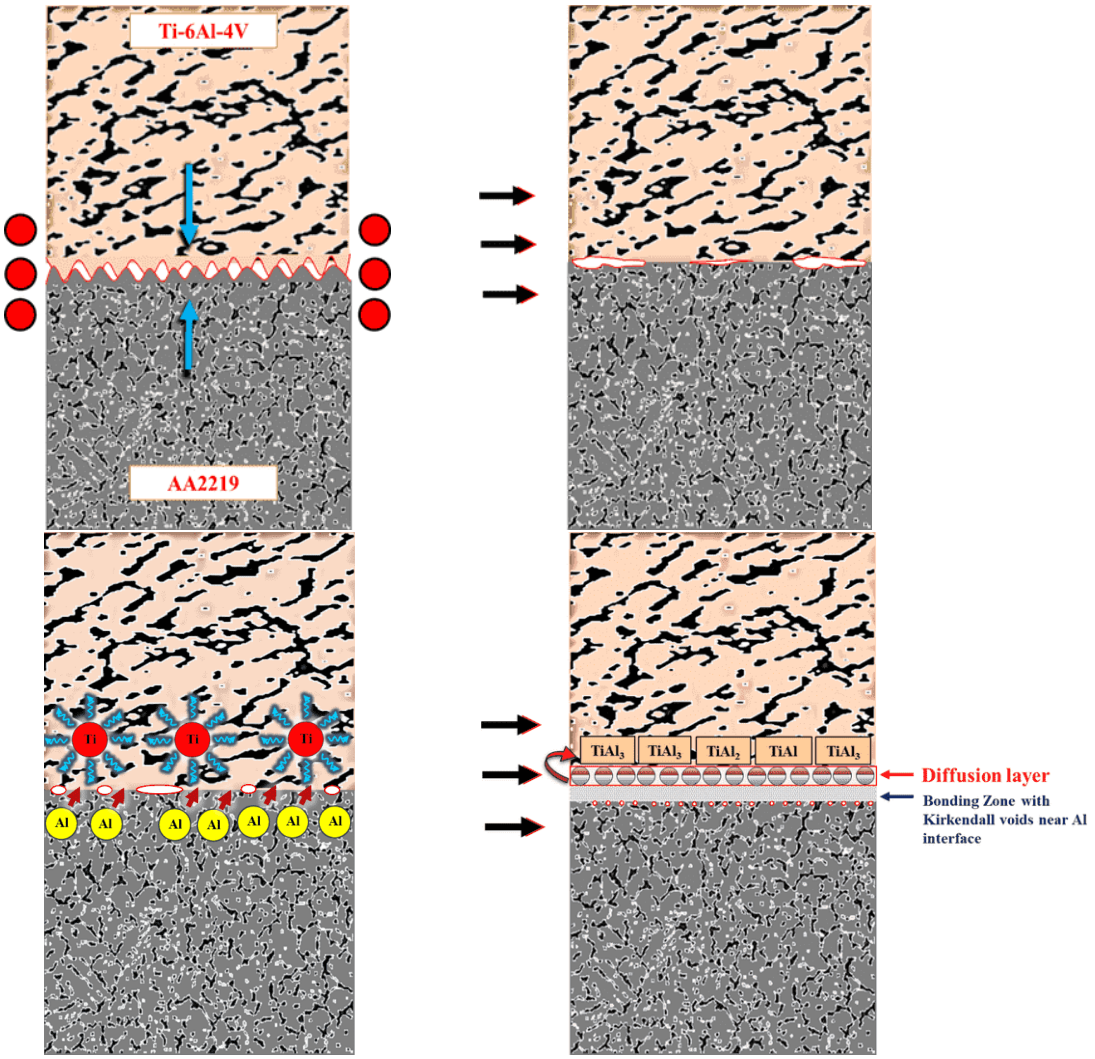

Fig. 11. Schematic for joint formation mechanism

[DOI: 10.22068/ijmse.3776]

In the reaction after the α-Al phase formation, the $TiAl_3$ intermetallic phase generates first, as the $TiAl_3$ has the lowest Gibbs free energy compared to the other phases. The TiAl and $TiAl_2$ phase originates in further reaction. However, the study did not find the Ti_3Al, Ti_2Al, Ti_3Al_5 and Ti_2Al_5 phases [47] at the interface.

5. CONCLUSIONS

The quality diffusion bonded joints of AA2219 and Ti-6Al-4V are successfully produced for various bonding pressures in the range of 1-4 MPa, keeping the bonding temperature and holding time constant. The following conclusions are drawn from the current study.

1. With the increase in bonding pressure, the shear strength of the resultant joint is increased, and the maximum shear strength of 81 MPa is achieved for the bonding pressure of 4 MPa. The shear specimens failed predominantly at Al and the intermetallic site formed at the Ti side, and the fractured surfaces show the presence of TiAl, $TiAl_2$, and $TiAl_3$ intermetallic compounds in XRD analysis.
2. The voids and cracks are closed at the higher bonding pressure of 4 MPa, forming a diffusion zone of 0.76 µm. The line scan EDS shows the improved diffusion behaviour across the interface of Al and Ti with increased bonding pressure.
3. Maximum hardness of 173.94 HV is tested on the bonding joint made at the bonding pressure of 4 MPa, and the hardness values decreased when tested towards the Al side and increased towards the Ti side.

6. ACKNOWLEDGMENT

The authors greatly acknowledge AICTE, New Delhi, for funding this research work, under the Research Promotion Scheme (Grant details: File No. 8-114/FDC/RPS (Policy-1)/2019-20).

REFERENCES

[1] Dursun, T. and Soutis, C., "Recent developments in advanced aircraft aluminium alloys". Mater. Des., 2014, 56, 862-871. https://doi.org/10.1016/j.matdes.2013.12.002.

[2] Heinz, A., Haszler, A., Keidel, C., Moldenhauer, S., Benedictus, R. and Miller, W. S., "Recent development in aluminium alloys for aerospace applications". Mater. Sci. Eng. A., 2000, 280, 102-107. https://doi.org/10.1016/S0921-5093(99)00674-7.

[3] Nayan, N., Singh, G., Baunthiyal, D., Murty, S. N., Prabhu, T. A. and Singh, S. K., "Mechanical properties of cryo-rolled aluminium alloy AA2219 at 300, 77 and 20 K". Mater. Sci. Eng. A., 2023, 881, 145399. https://doi.org/10.1016/j.msea.2023.145399.

[4] Elgallad, E. M., Zhang, Z. and Chen, X. G., "Effect of two-step aging on the mechanical properties of AA2219 DC cast alloy". Mater. Sci. Eng. A., 2015, 625, 213-220. https://doi.org/10.1016/j.msea.2014.12.002.

[5] Seshagiri, P. C., Nair, B. S., Reddy, G. M., Rao, K. S., Bhattacharya, S. S. and Rao, K. P., "Improvement of mechanical properties of aluminium–copper alloy (AA2219) GTA welds by Sc addition". St. W.J., 2008, 13, 146-158. https://doi.org/10.1179/174329308X283866.

[6] Arora, K. S., Pandey, S., Schaper, M. and Kumar, R., "Microstructure evolution during friction stir welding of aluminum alloy AA2219". J. Mater. Sci. Technol., 2010, 26, 747-753. https://doi.org/10.1016/S1005-0302(10)60118-1.

[7] Akca, E. and Gursel, A., "Joining of dissimilar metals by diffusion bonding: Titanium alloy with aluminum". Mater. Test., 2017, 59, 330-337. https://doi.org/10.3139/120.111006.

[8] Li, H., Yang, C., Sun, L. and Li, M., "Influence of pressure on interfacial microstructure evolution and atomic diffusion in the hot-press bonding of Ti-33Al-3V to TC17". J. Alloys Compd., 2017, 720, 131-138. https://doi.org/10.1016/j.jallcom.2017.05.239.

[9] Yılmaz, O., "Effect of welding parameters on diffusion bonding of type 304 stainless steel–copper bimetal". Mater. Sci. Technol., 2001, 17, 989-994. https://doi.org/10.1179/026708301101510831.

[10] Isa, M. S. M., Moghadasi, K., Ariffin, M. A., Raja, S., bin Muhamad, M. R., Yusof, F. and bin Ab Karim, M. S., "Recent research progress in friction stir welding of aluminium and copper dissimilar joint: a review". J. Mater. Res. Technol., 2021, 15, 2735-2780.

[DOI: 10.22068/ijmse.3776]

https://doi.org/10.1016/j.jmrt.2021.09.037.
[11] Elmer, J.W., Klingman, J. and Van Bibber, K., "Effect of surface condition and bonding pressure on quality of diffusion bonded high purity copper for linear collider accelerator structures". Sci. Technol. Weld. Join., 2001, 6, 268-272. https://doi.org/10.1179/136217101101538857.
[12] Guo, W., Xin, J., Hao, D., Ma, Y., Xiong, J., Li, J. and Feng, Q., "Diffusion bonding of nickel-based powder metallurgy superalloy FGH98 with pure nickel interlayer". J. Mater. Res. Technol., 2024, 30, 267-282. https://doi.org/10.1016/j.jmrt.2024.03.082.
[13] Gao, Q., Zhang, L. and Teng, A., "Diffusion bonding behaviour of Nb–Si and TiAl alloys by spark plasma sintering". J. Mater. Res. Technol., 2024, 28, 1803-1809. https://doi.org/10.1016/j.jmrt.2023.12.086.
[14] Chen, Y., Huang, Y., Han, L., Liu, D., Luo, L., Li, C. and Wang, Z., "High-strength vacuum diffusion bonding of Cu-plated, sandblasted W and CuCrZr alloy". J. Mater. Res. Technol., 2021, 15, 6260-6271. https://doi.org/10.1016/j.jmrt.2021.11.069.
[15] Masahashi, N. and Hanada, S., "Effect of pressure application by HIP on microstructure evolution during diffusion bonding". Mater. Trans., 2005, 46, 1651-1655. https://doi.org/10.2320/matertrans.46.1651.
[16] Xu, R., Zhu, Y., Li, B., Yang, H. and Zhang, C., "Interface behaviors and mechanical properties of diffusion bonded 45 steel/ additive manufactured 316L steel joints". J. Mater. Res. Technol., 2024, 30, 1279-1287. https://doi.org/10.1016/j.jmrt.2024.03.188.
[17] Fernandus, M. J., Senthilkumar, T., Balasubramanian, V. and Rajakumar, S., "Optimizing diffusion bonding parameters to maximize the strength of AA6061 aluminum and AZ61A magnesium alloy joints". Exp. Tech., 2014, 38, 21-36. https://doi.org/10.1111/j.1747-1567.2012.00815.x.
[18] AlHazaa, A., Haneklaus, N. and Almutairi, Z., "Impulse pressure-assisted diffusion bonding (IPADB): Review and outlook". Metals, 2021, 11, 323. https://doi.org/10.3390/met11020323.
[19] Peng, Y., Li, J., Li, Z., Guo, Z., Guo, W. and Xiong, J., "Modelling of bonding pressure based on the plastic deformation mechanism of interfacial voids closure in solid-state diffusion bonding". Mater. Des., 2024, 245, 113239. https://doi.org/10.1016/j.matdes.2024.113239.
[20] Ravisankar, B., Krishnamoorthi, J., Ramakrishnan, S. S. and Angelo, P. C., "Diffusion bonding of SU 263". J. Mater. Process. Technol., 2009, 209, 2135-2144. https://doi.org/10.1016/j.jmatprotec.2008.05.015.
[21] Gietzelt, T., Walter, M., Toth, V., Messerschmidt, F. and Blem, M., "Comprehensive study of the influence of the bonding temperature and contact pressure regimes during diffusion bonding on the deformation and mechanical properties of AISI 304". Adv. Eng. Mater., 2021, 23, 2100188. https://doi.org/10.1002/adem.202100188.
[22] Gietzelt, T., Toth, V. and Huell, A., "Diffusion bonding: influence of process parameters and material microstructure". Join. Technol., 2016, 195-216. https://doi.org/10.5772/64312.
[23] Rajakumar, S. and Balasubramanian, V., "Diffusion bonding of titanium and AA 7075 aluminum alloy dissimilar joints—process modeling and optimization using desirability approach". Int. J. Adv. Manuf. Technol., 2016, 86, 1095-1112. https://doi.org/10.1007/s00170-015-8223-7.
[24] Akca, E. and Gursel, A., "The effect of diffusion welding parameters on the mechanical properties of titanium alloy and aluminum couples". Metals, 2017, 7, 22. https://doi.org/10.3390/met7010022.
[25] Wei, Y., Aiping, W., Guisheng, Z. and Jialie, R., "Formation process of the bonding joint in Ti/Al diffusion bonding". Mater. Sci. Eng. A, 2008, 480, 456-463. https://doi.org/10.1016/j.msea.2007.07.027.
[26] Jiangwei, R., Yajiang, L. and Tao, F., "Microstructure characteristics in the interface zone of Ti/Al diffusion bonding". Mater. Lett., 2002, 56, 647-652. https://doi.org/10.1016/S0167-577X(02)00570-0.
[27] Venugopal, S., Seeman, M., Seetharaman, R. and Jayaseelan, V., "The effect of bonding process parameters on the microstructure and mechanical properties of AA5083 diffusion-bonded joints". Int. J. Light. Mater. Manuf., 2022, 5, 555-563. https://doi.org/10.1016/j.ijlmm.2022.07.003.

[DOI: 10.22068/ijmse.3776]

[28] Tang, B., Qi, X. S., Kou, H. C., Li, J. S. and Milenkovic, S., "Recrystallization behavior at diffusion bonding interface of high Nb containing TiAl alloy". Adv. Eng. Mater., 2016, 18, 657-664. https://doi.org/10.1002/adem.201500457.

[29] Takahashi, Y., Nakamura, T. and Nishiguchi, K., "Dissolution process of surface oxide film during diffusion bonding of metals". J. Mater. Sci., 1992. 27, 485-498. https://doi.org/10.1007/BF00543942.

[30] Sousa, B. C., Walde, C., Champagne Jr, V. K., Nardi, A. T., Sisson Jr, R. D. and Cote, D. L., "Rapidly solidified gas-atomized aluminum alloys compared with conventionally cast counterparts: implications for cold spray materials consolidation". Coatings, 2020, 10, 1035. https://doi.org/10.3390/coatings10111035.

[31] Lim, P. Y., She, P. L. and Shih, H. C., "Microstructure effect on microtopography of chemically etched α+β Ti alloys". Appl. Surf. Sci., 2006, 253, 449-458. https://doi.org/10.1016/j.apsusc.2005.12.107.

[32] Fan, H.J., Knez, M., Scholz, R., Hesse, D., Nielsch, K., Zacharias, M. and Gösele, U., "Influence of surface diffusion on the formation of hollow nanostructures induced by the Kirkendall effect: the basic concept". Nano Lett., 2007, 7, 993-997. https://doi.org/10.1021/NL070026P.

[33] Yuan, L., Xiong, J., Peng, Y., Li, Z. and Li, J., "Modelling void closure in solid-state diffusion bonding of TC4 alloy". Vacuum, 2020, 173, 109120. https://doi.org/10.1016/j.vacuum.2019.109120.

[34] Zhang, C., Li, H. and Li, M., "Detailed evolution mechanism of interfacial void morphology in diffusion bonding". J. Mater. Sci. Technol., 2016, 32, 259-264. https://doi.org/10.1016/j.jmst.2015.12.002.

[35] Vatnalmath, M., Auradi, V., Murthy, B. V. and Nagaral, M., "Influence of bonding temperature on solid-state diffusion bonded joints of AA2219 and Ti-6Al-4V dissimilar alloys—microstructure and mechanical characterisation". Weld. World, 2025, 69, 373-81. https://doi.org/10.1007/s40194-024-01863-w.

[36] Assari, A. H. and Eghbali, B., "Solid state diffusion bonding characteristics at the interfaces of Ti and Al layers". J. Alloys Compd., 2019, 773, 50-58. https://doi.org/10.1016/j.jallcom.2018.09.253.

[37] Kecskes, L. J., Qiu, X., Liu, R., Graeter, J. H., Guo, S. and Wang, J., "Combustion synthesis reaction behavior of cold-rolled Ni/Al and Ti/Al multilayers". Army Research Laboratory Report ARL-TR-5507; US Army Research Research Laboratory: Aberdeen Proving Ground, MD, USA, 2011. https://apps.dtic.mil/sti/tr/pdf/ADA548641 .pdf.

[38] Wan, Q., Li, F., Wang, W., Hou, J., Cui, W. and Li, Y., "Microstructure and properties of in situ Ti–Al intermetallic compound-reinforced Al matrix composites with dispersive distribution of core–shell-like structure". Compos. Adv. Mater., 2021, 30. https://doi.org/10.1177/26349833211006117.

[39] Liu, Z. W., Rakita, M., Han, Q. and Li, J. G., "A Developed Method for Fabricating In-Situ TiC p/Mg Composites by Using Quick Preheating Treatment and Ultrasonic Vibration". Metall. Mater. Trans. A, 2012, 43, 2116-2124. https://doi.org/10.1007/s11661-011-1041-0.

[40] Mishin, Y. and Herzig, C., "Diffusion in the Ti–Al system". Acta Mater., 2000, 48, 589-623. https://doi.org/10.1016/S1359-6454(99)00400-0.

[41] Kundu, J., Chakraborty, A. and Kundu, S., "Bonding pressure effects on characteristics of microstructure, mechanical properties, and mass diffusivity of Ti-6Al-4V and TiAlNb diffusion-bonded joints". Weld. World, 2020, 64, 2129-2143. https://doi.org/10.1007/s40194-020-00989-x.

[42] Wang, C., Li, X., Zhong, Z., Song, K., Wang, G., Zhou, W. and Wu, Y., "Microstructure and mechanical properties of W/steel joints diffusion bonded with Nb and Nb/Ni interlayers by spark plasma sintering". J. Adhes. Sci. Technol., 2020, 34, 2638-2651. https://doi.org/10.1080/01694243.2020.1781353.

[43] Li, P., Sun, H., Wang, S., Xia, Y., Dong, H., Wen, G. and Zhang, H., "Diffusion bonding of AlCoCrFeNi2.1 eutectic high entropy alloy to GH4169 superalloy". Mater. Sci. Eng. A, 2020, 793, 139843. https://doi.org/10.1016/j.msea.2020.139843.

[44] Balasubramanian, M., "Characterization of

[DOI: 10.22068/ijmse.3776]

diffusion-bonded titanium alloy and 304 stainless steel with Ag as an interlayer". Int. J. Adv. Manuf. Technol., 2016, 82, 153-162. https://doi.org/10.1007/s00170-015-7376-8.

[45] Song, Y. L., Dou, Z. H., Zhang, T. A., Liu, Y. and Wang, G. C., "First-principles calculation on the structural, elastic and thermodynamic properties of Ti-Al intermetallics". Mater. Res. Express, 2019, 6, 1065a4. https://doi.org/10.1088/2053-1591/ab3e11.

[46] Hosseini, S.R.E., Feng, K., Nie, P., Zhang, K., Huang, J., Chen, Y., Shu, D., Li, Z., Guo, B. and Xue, S., "Fracture surface characterization of laser welding processed Ti alloy to stainless steel joints". Weld. World, 2018, 62, 947-960. https://doi.org/10.1007/s40194-018-0586-6.

[47] Schuster, J. C. and Palm, M., "Reassessment of the binary aluminum-titanium phase diagram". J. Phase Equilib. Diffus., 2006, 27, 255-277. https://doi.org/10.1361/154770306X109809.

[DOI: 10.22068/ijmse.3776]